Engineering Fracture Mechanics Vol. 37, No. 1, pp. 43–57, 1990
Printed in Great Britain.

0013-7944/90 $3.00 + 0.00

PLANE-STRESS MIXED-MODE NEAR-TIP FIELDS IN ELASTIC PERFECTLY PLASTIC SOLIDS

P. DONG† and J. PAN
The University of Michigan, Department of Mechanical Engineering and Applied Mechanics, Ann Arbor, MI 48109, U.S.A.

Abstract—Within the context of the small-strain approach, the plane-stress mixed-mode near-tip fields of a stationary crack in an elastic perfectly plastic solid under small-scale yielding conditions are examined by finite element methods. The finite element results show that asymptotically at the crack tip two elastic sectors exist under near mode I mixed-mode loading conditions, and one elastic sector exists under near mode II mixed-mode loading conditions. The fully yielded near-tip field, plastically deformed at all angles, is obtained *only* under pure mode II loading conditions. The corresponding asymptotic crack-tip solutions (consisting of constant stress sectors, curved fan sectors, and elastic sectors) are also constructed. The asymptotic crack-tip stress solutions agree well with the finite element results for the complete range of mixed-mode loadings. Some similarities and differences between the near-tip fields under plane-stress and plane-strain conditions are also discussed.

1. INTRODUCTION

A SUBSTANTIAL understanding of the near-tip structures for power-law hardening materials obeying a deformation plasticity theory has been achieved in recent years. Representative works along this line are those of Hutchinson[1, 2], Rice[3], and Rice and Rosengren[4] for a crack under pure mode I and pure mode II loading conditions, and of Shih[5, 6] under mixed-mode loading conditions. For power-law hardening materials, the asymptotic crack-tip stress and strain fields possess the well-known HRR singularity. The corresponding crack-tip field solutions for perfectly plastic materials were also proposed by the above authors, with the assumption that the material surrounding the crack-tip is fully yielded at all angles. These solutions agree with the perfectly plastic limits of the corresponding asymptotic solutions for power-law hardening materials, and contain radial stress discontinuities under plane-strain near mode I mixed-mode conditions and under plane-stress mode I and mixed-mode conditions (for anisotropic perfectly plastic materials, see Pan[7, 8]).

Within the framework of rigid perfectly plastic theory (where the elastic strain is neglected), a line of discontinuity in the stress field may be viewed as a mathematical idealization of an infinitively thin elastic region separating two plastic regions. However, for perfectly plastic materials when the material elasticity is considered, it seems reasonable to ask: how does the elastic strain affect the near-tip field structures?

To address the above issue under plane-strain conditions, Gao[9] proposed the crack-tip stress fields that contain two elastic sectors under mixed-mode loading conditions. However, the finite element computations carried out by Saka *et al.*[10] showed that only one elastic sector exists around the crack tip under mixed-mode loading and small-scale yielding conditions, with Poisson's ratio being nearly 1/2. A systematic investigation of the plane-strain mixed-mode crack-tip fields has been conducted by Dong and Pan[11, 12]. Their computational results and asymptotic analysis show that, as the limiting steady-stress state near the crack tip, the near mode I crack-tip fields do contain an elastic sector, but they differ from the crack-tip fields proposed by Saka *et al.*[10] by a constant stress sector separating the elastic sector and a neighboring fan sector. The corresponding conditions for the existence of the elastic sector were examined by asymptotic analyses and verified by finite element computations.

Very little information is available in the literature pertaining to the above issues for elastic perfectly plastic materials, particularly under plane-stress mixed-mode loading conditions, despite its practical importance to structural problems. To our best knowledge, a detailed finite

†Current address: Edison Welding Institute, Columbus OH 43220, U.S.A.

element investigation of the near-tip fields for elastic perfectly plastic materials under plane-stress and small-scale yielding conditions was done by Narasimhan and Rosakis[13] for pure mode I loading. However, the two constant stress sectors of the asymptotic near-tip field assembled by Hutchinson[2] were not identified in their investigations. Thus, detailed numerical work as well as the corresponding asymptotic analyses are required to firmly establish a conceptual understanding of near-tip behaviors under plane-stress conditions. This is usually more complex than that in plane-strain because the equations of plane-stress perfect plasticity are somewhat more involved[14].

In this paper, the plane-stress small-scale yielding near-tip fields under monotonically increasing mixed-mode loading are examined using finite element methods. The material is assumed to be an elastic perfectly plastic solid obeying the J_2 flow theory. Attempts are made to elucidate the details of the limiting stress states near a crack tip, which we will refer to as the steady stress states. Then, the asymptotic near-tip fields for elastic perfectly plastic solids are assembled and shown to be in excellent agreement with the finite element results.

2. FINITE ELEMENT ANALYSIS

2.1. *Computational model*

We consider a crack in an elastic perfectly plastic solid with the reference coordinate systems depicted in Fig. 1; the Cartesian coordinates x_1 and x_2 and the polar coordinates r and θ are centered at the tip. The mixed-mode small-scale yielding problem was modelled by considering the crack in the circular domain of radius r_o, as shown. The circular domain was entirely discretized by finite elements. In the immediate crack-tip region, we used a ring of 40 wedge-shaped elements of size r_i. Collapsed nodes were employed to simulate the $1/r$ singularity in strain at the tip. The crack-tip elements were equally distributed from $-\pi$ to π and surrounded by 24 circular strips of elements generated by a logarithmic scale in the r direction. The entire model consists of a total of 1000 isoparametric elements, and $r_i/r_o \approx 10^{-7}$ is used in the calculations.

The displacements due to the leading singular terms of the linear elastic asymptotic solution of the crack-tip field,

$$u_i = \frac{1}{2G}\sqrt{\frac{r}{2\pi}}\,(K_{\mathrm{I}}\hat{u}_i(\theta, \nu)^{\mathrm{I}} + K_{\mathrm{II}}\hat{u}_i(\theta, \nu)^{\mathrm{II}}), \quad i = 1, 2, \tag{1}$$

are specified as the boundary conditions at the outermost boundary $r = r_0$ of the domain. Here, G represents the shear modulus, ν represents the Poisson ratio, K_{I} and K_{II} denote the mode I and mode II stress intensity factors of the far-field, and $\hat{u}_i(\theta, \nu)^{\mathrm{I}}$ and $\hat{u}_i(\theta, \nu)^{\mathrm{II}}$ are the dimensionless

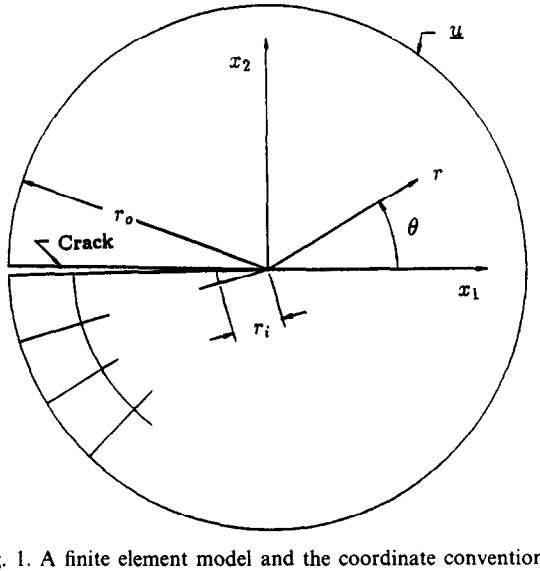

Fig. 1. A finite element model and the coordinate conventions.

displacement functions associated with the elastic singularity and depend only on the orientation θ for a given elastic material. The loading is applied through the stress intensity factors, K_I and K_{II}, which are the amplitude factors in eq. (1). The relative composition of K_I and K_{II} is controlled through a mixity factor M^e, defined as[5]

$$M^e = \frac{2}{\pi} \arctan\left[\lim_{r\to\infty} \frac{\sigma_{\theta\theta}(r, \theta = 0)}{\sigma_{r\theta}(r, \theta = 0)}\right]$$

$$= \frac{2}{\pi} \arctan\left[\frac{K_I}{K_{II}}\right], \tag{2}$$

where the magnitude of M^e ranges from 0 to 1, with $M^e = 0$ for pure mode II, and $M^e = 1$ for pure mode I.

Eight-node serendipity elements with a reduced integration scheme were used in the element stiffness calculations. In a previous article[12], we showed that both eight-node serendipity elements with a reduced integration scheme and nine-node Lagrangian elements with the $\bar{B}$-method proposed by Hughes[15] can be effectively used to relieve the artificial mesh-locking that occurs for nearly incompressible materials in plane strain. However, this problem does not arise in plane-stress since there is a non-zero out-of-plane strain component that is determined in terms of the in-plane strain components.

2.2. *Numerical procedure*

The material was modelled as an elastic perfectly plastic solid. A small-strain incremental plasticity theory was employed with the Huber–Von Mises yield condition and the associated flow rule. A displacement-based finite element method with an iterative procedure based on a modified Newton–Raphson method was used in the analysis. The finite element equations were derived from the principle of virtual work. At time $t + \Delta t$, this takes the form

$$\int_A \sigma_{ij}(t + \Delta t)\, \delta\epsilon_{ij}\, \mathrm{d}A = \int_{\partial A} T_i(t + \Delta t)\, \delta u_i\, \mathrm{d}S, \tag{3}$$

where $\sigma_{ij}(t + \Delta t)$ represents the Cauchy stress tensor, which satisfies the equilibrium conditions at time $t + \Delta t$, and $T_i(t + \Delta t)$ is the imposed traction vector on the boundary ∂A of domain A. In addition, δu_i represents the virtual displacement field that vanishes on the part of the boundary where displacements are specified, and $\delta\epsilon_{ij}$ is the associated small-strain tensor. Here, time t is used as a convenient variable to represent differential loading levels. Linearizing eq. (3) with respect to the equilibrium configuration at time t and introducing the finite element approximation, we obtain the following incremental equilibrium equations in matrix notation:

$$\mathbf{K}_T \Delta\mathbf{U} = \mathbf{F}(t + \Delta t) - \mathbf{P}(t), \tag{4}$$

where $\Delta\mathbf{U} = \mathbf{U}(t + \Delta t) - \mathbf{U}(t)$ is the vector of incremental displacements at the nodal points, $\mathbf{K}_T = \int_A \mathbf{B}^T\mathbf{D}\mathbf{B}\, \mathrm{d}A$ is the tangent stiffness matrix corresponding to the configuration at time t ($\mathbf{B}$ is the strain–displacement matrix and $\mathbf{D}$ the material constitutive matrix of the elastic–plastic material), $\mathbf{F}(t + \Delta t)$ is the vector of the applied external loads at time $t + \Delta t$, and $\mathbf{P}(t) = \int_A \mathbf{B}\sigma(t)\, \mathrm{d}A$ is the equivalent force vector of the element stresses at time t.

The loading is applied through the mode I and the mode II stress intensity factors, which enter the far-field displacement boundary conditions [eq. (1)]. The remote load intensity can be expressed in terms of the well-known J integral[3],

$$J = \frac{1}{E}(K_I^2 + K_{II}^2), \tag{5}$$

in order to facilitate subsequent discussions. A small initial load (small J) is applied so that all elements remain elastic. J is then scaled to cause incipient yielding at the crack-tip element where

the stresses are the highest. At this point the value of J is denoted as J_0. The load is then increased incrementally by a fraction of J_0. An iterative Newton–Raphson procedure is employed to solve the incremental equilibrium equations (eq. 4) for each load increment, such that for the kth equilibrium iteration at time $t + \Delta t$, the Euclidean norm

$$\Delta \mathbf{R}^k = \mathbf{F}(t + \Delta t) - \mathbf{P}^{k-1}(t + \Delta t) \tag{6}$$

satisfies

$$\frac{\|\Delta \mathbf{R}^k\|}{\|\mathbf{F}\|} \leqslant TOL, \tag{7}$$

where the TOL is a small preset tolerance. It is important that the stress evaluation, which can be written as

$$\sigma_{ij}^k(t + \Delta t) = \sigma_{ij}(t) + \int_{\epsilon_{ij}(t)}^{\epsilon_{ij}^k(t+\Delta t)} D_{ijkl}\, \mathrm{d}\epsilon_{kl}, \tag{8}$$

is performed by integrating from the values of the last accepted equilibrium state to the current state of iteration k, so that the final results are not affected by errors introduced during intermediate iterations[16]. The incremental processes are continued until a steady stress state at the crack tip is observed. At all times the maximum extent of the plastic zone around the crack tip is smaller than 1/100 of r_0 to preserve small-scale yielding conditions[11]. For the results reported here, Poisson's ratio ν is taken as 0.3, and the ratio of Young's modulus E to the tensile yield stress σ_0 (E/σ_0) as 500 to represent typical structural steels.

2.3. *Numerical results*

The crack tip stress fields at $r/r_p \approx 10^{-2}$ for various combinations of K_{I} and K_{II} of the far-field are shown in Fig. 2 for near mode I mixed-mode loadings ($M^e = 1$, 0.84, and 0.54), and in Fig. 3 for near mode II mixed-mode loadings ($M^e = 0.30$, 0.15, and 0). Here r_p represents the extent of the plastic zone from the crack tip at $\theta = 0$. In these figures, $\sigma_e (= \frac{3}{2} s_{ij} s_{ij}$, where s_{ij} is the deviatoric stress) represents the effective stress, and only every other data point is plotted for clarity. No smoothing techniques were used in any manner in displaying the numerical results. The symbols are the finite element results taken directly from the Gauss quadrature points in the immediate vicinity of the crack-tip, after the steady stress state is observed. (Note that the stress components shown in all the figures in this paper are normalized by the yield stress σ_0.)

In all the cases, the stress fields contain no discontinuities in the radial stress component, σ_{rr}, in contrast to the asymptotic solutions constructed by Shih[6] and Dong and Pan[14], where it was assumed that the material surrounding the crack tip is fully yielded. It can be seen that σ_e is less than unity in the two regions bordering the two crack faces for near mode I mixed-mode loadings [Fig. 2(a–c)], and in the region bordering the lower crack surface for near mode II mixed-mode loadings [Fig. 3(a, b)]. For pure mode I, similar results were also reported by Narasimhan and Rosakis[13]. It should be noted that the fully yielded crack-tip stress field is obtained *only* under pure mode II conditions [Fig. 3(c)]. A careful examination of Fig. 3(b) shows that in the neighborhood of the lower crack face ($\theta = -180°$) σ_e is less than unity, and it is still deformed elastically.

In Fig. 4(a, b), we plot the normalized stresses with respect to the normalized radial distance from the crack tip, r/r_p, in a logarithmic scale along two radial lines for $M^e = 0.54$. One radial line is within the elastic sector at $\theta = 133°$, and the other is well inside the plastically deformed region at $\theta = 7.1°$. In both figures, we see that for $r/r_p > 1$, the straight line distributions of the normalized stresses as functions of the normalized radial distance have a slope of $-1/2$ and clearly indicate the $r^{-\frac{1}{2}}$ singularity as it must be in the elastic K-field. As r/r_p approaches 1, the magnitude of the slope decreases. As r/r_p decreases from 1, the slope of these lines becomes zero inside the plastically deformed region [Fig. 4(b)] and becomes zero at $r/r_p \approx 10^{-1}$ within the elastic sector [Fig. 4(a)].

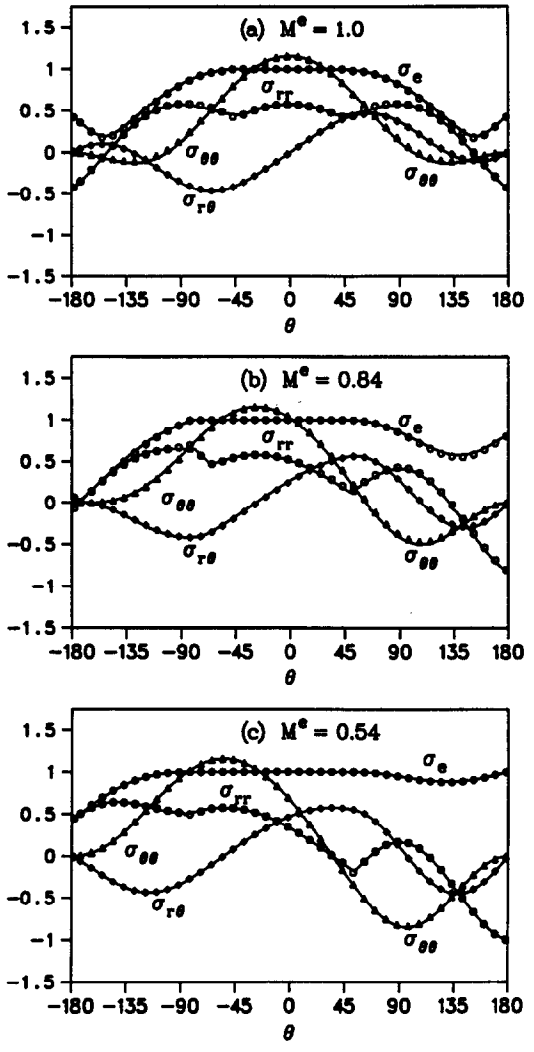

Fig. 2. Comparisons of the finite element results with the asymptotic solutions for near mode I mixed-mode loadings: (a) $M^e = 1$ (mode I), (b) $M^e = 0.84$, (c) $M^e = 0.54$.

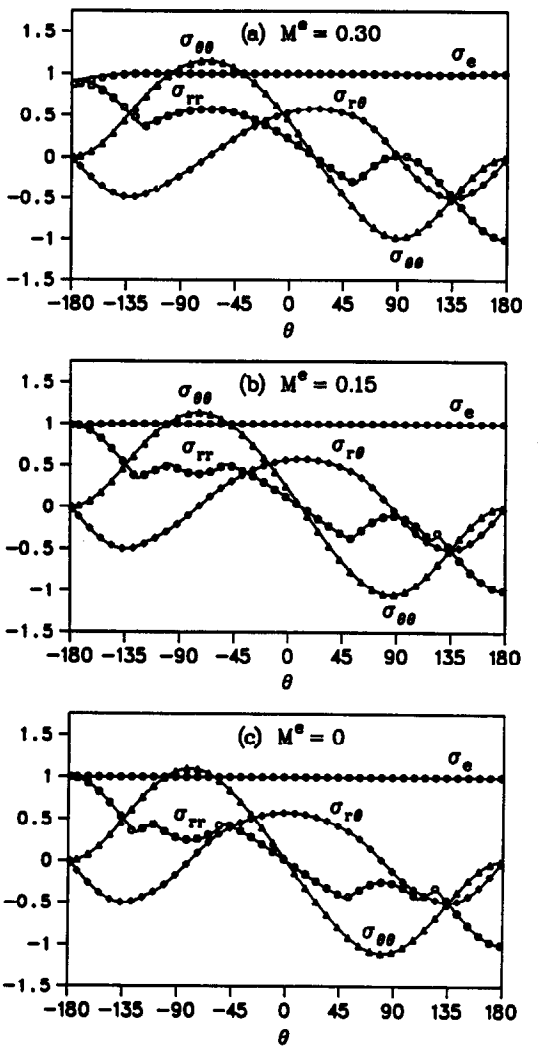

Fig. 3. Comparisons of the finite element results with the asymptotic solutions for near mode II mixed-mode loadings: (a) $M^e = 0.30$, (b) $M^e = 0.15$, (c) $M^e = 0$ (mode II).

To facilitate direct comparisons between the finite element solutions and the asymptotic solutions presented in the next section, we introduce a near-field mixity parameter M^p. This parameter M^p, defined by Shih[5], identifies each stress field in Fig. 2 and Fig. 3 by the relative composition of mode I and mode II conditions directly ahead of the tip. Thus, the near-field mixity parameter, M^p, can be expressed in the same way as M^e in eq. (2) in terms of the opening stress and the shear stress ahead of the crack tip:

$$M^p = \frac{2}{\pi} \arctan\left[\lim_{r \to 0} \frac{\sigma_{\theta\theta}(r, \theta = 0)}{\sigma_{r\theta}(r, \theta = 0)}\right]. \tag{9}$$

The magnitude of M^p equals 1 for pure mode I and 0 for pure mode II. The value of M^p lies between 1 and 0 for mixed-mode loading. For a given far-field mixity parameter M^e, defined by eq. (2), there exists a unique value of M^p under the prescribed loading conditions. The relationship between M^e and M^p is plotted in Fig. 5 from the current finite element computations.

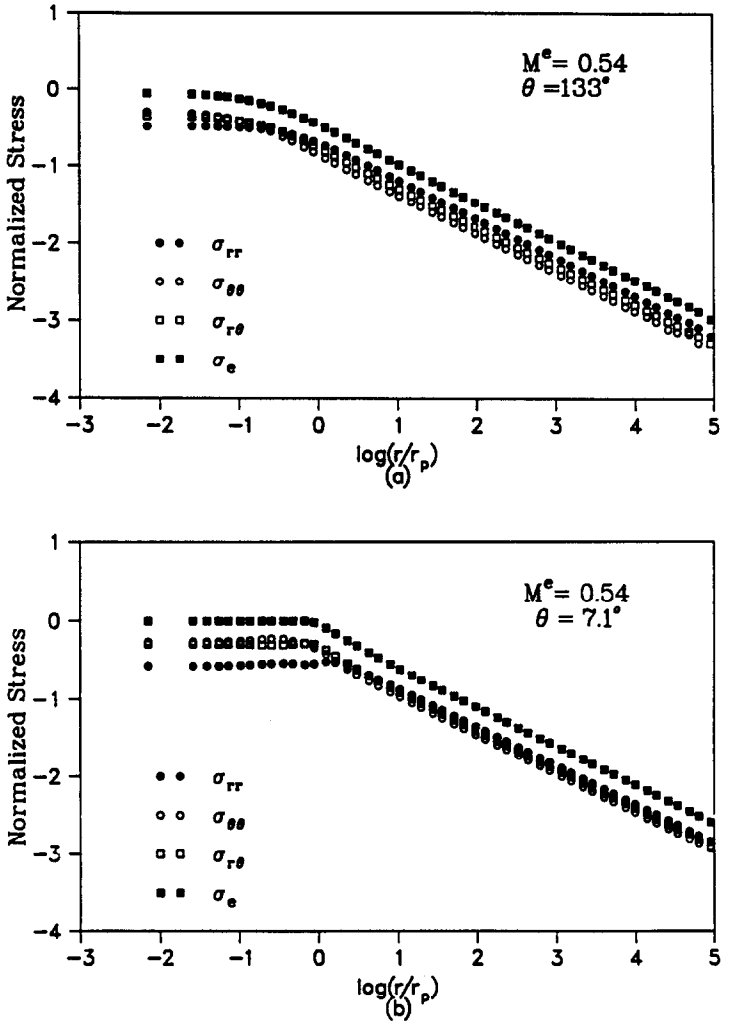

Fig. 4. Log–log plots of the normalized stresses as functions of the normalized radial distance for $M^e = 0.54$ at two angles: (a) $\theta = 133°$ (inside the elastic region), (b) $\theta = 7.1°$ (inside the plastically deformed region).

3. ASYMPTOTIC NEAR-TIP FIELDS

3.1. *Equilibrium equations*

In this and subsequent sectors, we intend to seek a near-tip solution in which all stresses are continuous. With reference to the polar coordinates (see Fig. 1), the equilibrium equations can be written as

$$\frac{\partial \sigma_{rr}}{\partial r} + \frac{1}{r}\frac{\partial \sigma_{r\theta}}{\partial \theta} + \frac{\sigma_{rr} - \sigma_{\theta\theta}}{r} = 0. \tag{10}$$

$$\frac{1}{r}\frac{\partial \sigma_{\theta\theta}}{\partial \theta} + \frac{\partial \sigma_{r\theta}}{\partial r} + \frac{2\sigma_{r\theta}}{r} = 0. \tag{11}$$

Rice[3, 17] analysed the stress state $\sigma_{ij} = \sigma_{ij}(\theta)$ as $r \to 0$ at the tip of a stationary crack and a growing crack in an elastic perfectly plastic solid. He argued that since the stress at the tip must be bounded, terms of the form $r(\partial \sigma_{ij}/\partial r)$ in the equilibrium equations must vanish as $r \to 0$. Hence, eqs (10) and (11) reduce to the two ordinary differential equations:

$$\sigma_{rr} - \sigma_{\theta\theta} + \frac{d\sigma_{r\theta}}{d\theta} = 0, \tag{12}$$

$$2\sigma_{r\theta} + \frac{d\sigma_{\theta\theta}}{d\theta} = 0. \tag{13}$$

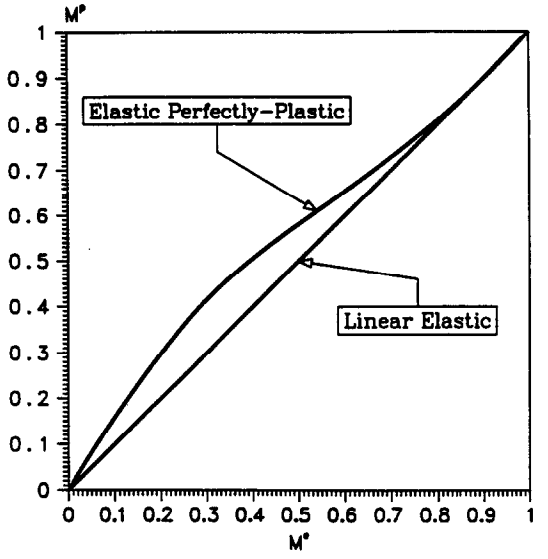

Fig. 5. Relationship between the near-field plastic mixity M^p and the far-field elastic mixity M^e obtained from the finite element analysis.

3.2. *Yield condition*

Following the development of Rice[17], we write the J_2 yield condition as

$$\Phi(\sigma_{ij}) = \tfrac{3}{2}s_{ij}s_{ij} - \sigma_0^2 = 0, \tag{14}$$

where s_{ij} is the deviatoric part of σ_{ij}, and σ_0 is the tensile yield stress. Under plane-stress conditions, the yield condition (14) is expressed as

$$\Phi(\sigma_{ij}) = \sigma_{11}^2 + \sigma_{22}^2 - \sigma_{11}\sigma_{22} + 3\sigma_{12}^2 - \sigma_0^2 = 0, \tag{15}$$

referring to the Cartesian coordinates, and

$$\Phi(\sigma_{ij}) = \sigma_{rr}^2 + \sigma_{\theta\theta}^2 - \sigma_{rr}\sigma_{\theta\theta} + 3\sigma_{r\theta}^2 - \sigma_0^2 = 0, \tag{16}$$

referring to the polar coordinates. The differential form of the yield condition, as r approaches 0, is

$$s_{ij}\frac{\mathrm{d}\sigma_{ij}}{\mathrm{d}\theta} = 0. \tag{17}$$

Under plane-stress conditions, eq. (17), in combination with the equilibrium equations (12) and (13), gives

$$\frac{\mathrm{d}(\sigma_{11} + \sigma_{22})}{\mathrm{d}\theta}s_{rr} = 0. \tag{18}$$

3.3. *Plastic crack-tip sectors*

Equation (18) leads to the following forms of simple solutions near the tip:

(*i*) *Constant stress sectors.* Within a constant stress sector, the stresses σ_{11}, σ_{22}, and σ_{12} (referring to the Cartesian coordinates) are independent of θ, i.e.

$$\sigma_{11} = constant, \tag{19}$$

$$\sigma_{22} = constant, \tag{20}$$

$$\sigma_{12} = constant, \tag{21}$$

where the constants are chosen to satisfy the yield condition and other relevant boundary conditions. The characteristic grid is generated by two non-orthogonal families of parallel lines [see Fig. 6(a)]. The angle 2ψ is a function of σ_{11}, σ_{22}, and σ_{12}.

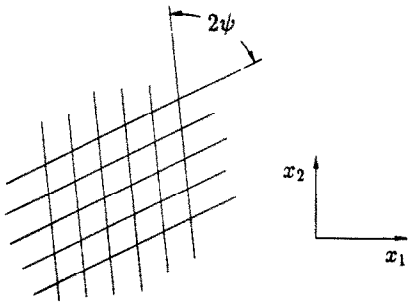

(a)

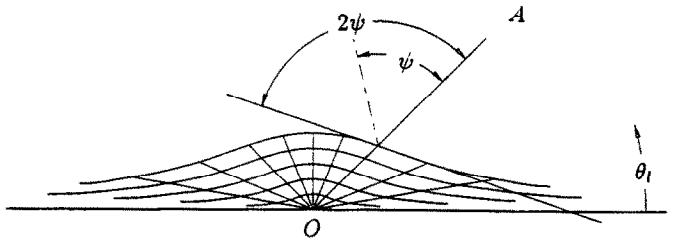

(b)

Fig. 6. Asymptotic crack-tip sectors: (a) constant stress sector, (b) curved fan sector (fully extended).

(*ii*) *Curved fan sectors.* Within a curved fan sector, $s_{rr} = 0$ corresponds to one of two families of characteristics, namely, a fan of radial lines. Along these radial lines,

$$\sigma_{\theta\theta} = 2\sigma_{rr}. \tag{22}$$

The equilibrium equations (12) and (13) and the yield condition (16) are satisfied if we take

$$\sigma_{rr} = \pm\tau_0 \cos\theta_l, \tag{23}$$

$$\sigma_{\theta\theta} = \pm 2\tau_0 \cos\theta_l, \tag{24}$$

$$\sigma_{r\theta} = \pm\tau_0 \sin\theta_l, \tag{25}$$

where $\tau_0 (= \sigma_0/\sqrt{3})$ is the yield stress in shear, and θ_l is measured counterclockwise, as shown in Fig. 6(b) for a fully-expanded curve fan sector. Evidently, the stresses are constant along the radial lines. As shown in Dong and Pan[14], the equation for the curved characteristics has the following form:

$$r^2 \sin\theta_l = constant. \tag{26}$$

The curved characteristics tend asymptotically to the horizontal line at $\theta_l = 0$ and π. Along this horizontal line the two families of the characteristics converge to one, and $\sigma_{\theta\theta} = \pm 2\tau_0$, $\sigma_{rr} = \pm\tau_0$. Both the stress states correspond to the parabolic points at the Von Mises ellipse[18]. Hill[19] has shown that at the parabolic point $\sigma_{\theta\theta} = 2\tau_0$ and $\sigma_{rr} = \tau_0$, the normal velocity component has a discontinuity and thinning occurs along the line of discontinuity, and that at $\sigma_{\theta\theta} = -2\tau_0$ and $\sigma_{rr} = -\tau_0$, the normal velocity component has a discontinuity, but thickening occurs.

3.4. *Elastic crack-tip sectors*

As seen in the finite element results, it seems reasonable to admit the existence of an elastic region around the crack tip and to assume that the stresses in the elastic region are nonsingular. For the elastically deformed region, the compatibility equation in terms of stress components gives

$$\nabla^2(\sigma_{rr} + \sigma_{\theta\theta}) = 0, \tag{27}$$

where ∇^2 is the Laplace operator with respect to the polar coordinate system, i.e.

$$\nabla^2 = \frac{\partial^2}{\partial r^2} + \frac{1}{r}\frac{\partial}{\partial r} + \frac{1}{r^2}\frac{\partial^2}{\partial \theta^2}, \tag{28}$$

and its corresponding asymptotic form for bounded stresses as $r \to 0$ is

$$r^2\left(\frac{\partial^2}{\partial r^2} + \frac{1}{r}\frac{\partial}{\partial r} + \frac{1}{r^2}\frac{\partial^2}{\partial \theta^2}\right) \to \frac{\partial^2}{\partial \theta^2}. \tag{29}$$

Then, the compatibility eq. (27) becomes an ordinary differential equation:

$$\frac{d^2}{d\theta^2}(\sigma_{rr} + \sigma_{\theta\theta}) = 0. \tag{30}$$

Solving eqs (12), (13) and (30), we can write the solutions for the stress components in the following forms:

$$\sigma_{rr} = 2A + 2B\theta - 2C\cos 2\theta - 2D\sin 2\theta, \tag{31}$$

$$\sigma_{\theta\theta} = 2A + 2B\theta + 2C\cos 2\theta + 2D\sin 2\theta, \tag{32}$$

$$\sigma_{r\theta} = -B + 2C\sin 2\theta - 2D\cos 2\theta. \tag{33}$$

The integration constants A, B, C, and D are to be determined by the boundary conditions.

3.5. *Assembly of the crack-tip solutions*

The possible crack-tip sectors categorized in the previous sections may be assembled in a manner that is consistent with the continuity of σ_{rr}, $\sigma_{r\theta}$, and $\sigma_{\theta\theta}$, since we seek a solution in which all the stresses are continuous. (Note that the traction continuity across a radial line emanating from the crack tip requires the continuity of $\sigma_{\theta\theta}$ and $\sigma_{r\theta}$, but not σ_{rr}.) The assemblies of the crack-tip fields are shown in Figs 7 and 8 in the order of departure from pure mode I to pure mode II.

3.5.1. *Near mode I* ($M^p = 1$–0.392)

For near-mode I mixed-mode loading, the finite element results suggest the solution shown in Fig. 7(b) as a possibility. Regions (1) and (5) are elastic sectors, (2) and (4) curved fan sectors, and (3) a constant stress sector. Detailed examinations of this solution show that such a near-tip field does not exist for the entire range of near mode I mixed-mode loading unless a trace of a constant stress sector, as shown in Fig. 7(c), intervenes between regions (1) and (2) of Fig. 7(b). In what follows, we discuss the two types of the near-tip fields separately.

(*i*) *Solution* 1. In Fig. 7(b), the parameters δ, δ_1, and θ_1 through θ_6 are defined in the same fashion as in Dong and Pan[14]. The two radial lines oO and oO' are the asymptotes of the curved characteristics of fan sectors (2) and (4), respectively. The stresses in the two elastic sectors, (1) and (5), are given by eqs (31)–(33), the stresses in the two curved fan sectors by eqs (23)–(25), and the stresses in the constant stress sector by eqs (19)–(21). The continuity requirements across a radial line between any two adjacent sectors and the traction-free boundary conditions along the crack surfaces generate thirteen equations in terms of fourteen undetermined parameters. The parameter δ and the near-field mixity M^p is related by

$$M^p = \frac{2}{\pi}\arctan\left[\frac{2}{\tan\delta}\right], \tag{34}$$

as shown in Dong and Pan[14]. As δ varies from 0° (mode I) to 90° (mode (II), M^p varies from 1 to 0. For a given far-field mixity, M^e, the corresponding near-tip mixity, M^p, can be found in Fig. 5. Then, the parameter δ is prescribed by eq. (34). For a given value of δ, the thirteen equations can be solved using a simple numerical procedure. To examine the existence of such a solution, however, we only need to analyse the elastic sector, region (1), in detail.

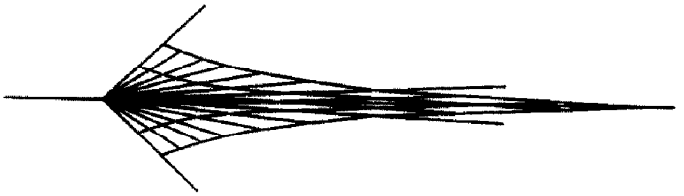

(a)

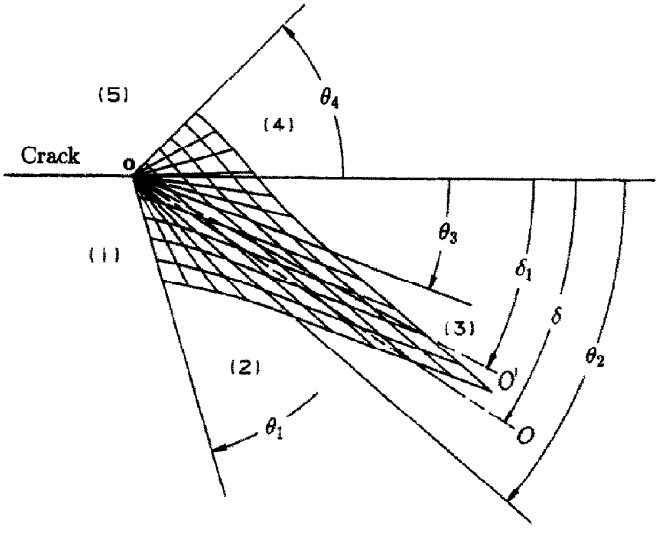

(b)

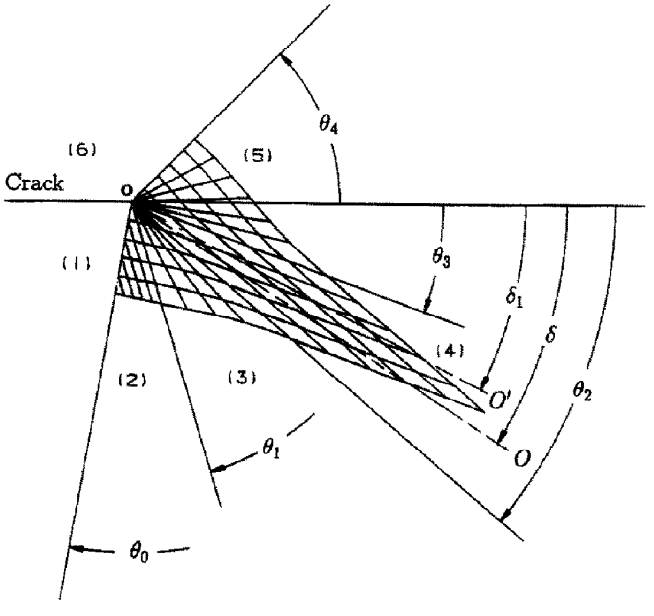

(c)

Fig. 7. Assembly of the crack-tip solutions under near mode I mixed-mode loadings: (a) mode I limit of solution 1, (b) solution 1, (c) solution 2.

Within the elastic sector, region (1), the integration constants can be expressed as

$$A = \frac{1}{8}\frac{\tau_0 \cos(\theta_1 + \delta_1)(6\pi \cos 2\theta_1 - 3 \sin 2\theta_1 - 2\theta_1)}{2\pi \cos 2\theta_1 - \sin 2\theta_1 + 2\theta_1 \cos 2\theta_1}, \tag{35}$$

$$B = \frac{1}{2}\frac{\tau_0 \cos(\theta_1 + \delta_1)(1 + 3 \cos 2\theta_1)}{2\pi \cos 2\theta_1 - \sin 2\theta_1 + 2\theta_1 \cos 2\theta_1}, \tag{36}$$

$$C = \frac{1}{8}\frac{\tau_0 \cos(\theta_1 + \delta_1)(4\pi + 6\pi \cos 2\theta_1 + 3 \cos 2\theta_1 + 2\theta_1)}{2\pi \cos 2\theta_1 - \sin 2\theta_1 + 2\theta_1 \cos 2\theta_1}, \tag{37}$$

$$D = -\frac{1}{4}\frac{\tau_0 \cos(\theta_1 + \delta_1)(1 + 3 \cos 2\theta_1)}{2\pi \cos 2\theta_1 - \sin 2\theta_1 + 2\theta_1 \cos 2\theta_1}, \tag{38}$$

where θ_1 must satisfy the following equation:

$$\frac{2(1 + \cos 2\theta_1)(\cos 2\theta_1 - 1)}{2\pi \cos 2\theta_1 - \sin 2\theta_1 + 2\theta_1 \cos 2\theta_1} + \frac{4\pi + 6\pi \cos 2\theta_1 + 3 \cos 2\theta_1 + 2\theta_1)}{2\pi \cos 2\theta_1 - \sin 2\theta_1 + 2\theta_1 \cos 2\theta_1} = 4 \tan(\theta_1 + \delta_1). \tag{39}$$

Before eq. (39) can be solved for θ_1, the parameter δ_1 needs to be determined. This cannot be done unless all thirteen equations are solved simultaneously at a given δ. Nevertheless, for a solution to be physically valid, $\delta_1 \leqslant \delta$ must always be true as δ varies between 0° and 90°. A simple numerical procedure is employed to solve eq. (39) for θ_1 at a given δ_1.

For pure mode I loading (the mode I limit of the mixed-mode cases), $\delta_1 = -\delta = 0.013°$, $\theta_1 = -\theta_4 = -39.29°$ and $\theta_2 = -\theta_3 = 1.83°$. The corresponding stress field is displayed as the solid lines in Fig. 2(a). The agreement between the analytical solution and the finite element results is evident. The symmetric mode I characteristic field near the crack tip is sketched in Fig. 7(a) (θ_2 and θ_3 are exaggerated in this sketch for clarity), and it can be regarded as the special case of the mixed-mode field shown in Fig. 7(b). However, for near mode I mixed-mode loading, surprisingly enough, solution 1 exists only for a very small range of mixed-mode loadings when $0.013° \leqslant \delta_1 < 3°$. No such solution for the characteristic field shown in Fig. 7(b) exists when $3° \leqslant \delta_1 \leqslant 58°$, which virtually spans the entire range of the near mode I mixed-mode loading. In order to guarantee a solution (regardless of whether or not it is feasible), a trace of a constant stress sector must intervene between regions (1) and (2); thus, solution 1 [Fig. 7(b)] may be viewed as a special case of the resulting near-tip field shown in Fig. 7(c) in which the constant stress sector [region (2)] becomes negligibly small.

(*ii*) *Solution* 2. A partial constant stress sector [see Fig. 7(c)] is introduced between regions (1) and (2). The new near-tip field, then, involves fifteen unknown parameters with fourteen equations being available. Attempts to find another equation were unsuccessful. For comparison purposes, θ_0 from the finite element computations is used instead to construct the analytical solutions. Two solutions for the near-tip stress fields at $M^p = 0.85$ and $M^p = 0.61$ are displayed as the solid lines against the corresponding finite element results in Fig. 2(b, c). As θ_4 approaches 54.74°, the elastic sector (6) becomes a plastic constant stress sector and region (2) [in Fig. 7(c)] becomes hardly noticeable. At this point, δ is 70.53° ($M^p = 0.392$). The corresponding characteristic field is shown in Fig. 8(a), and the stress field is shown as the solid lines in Fig. 3(a). The finite element results in Fig. 3(a) ($M^e = 0.30$) clearly show that this is exactly the case.

3.5.2. *Near mode II* ($M^p = 0.392$–0)

As δ deviates further from mode I (δ increases from 70.53°), a curved fan sector develops between regions (5) and (6) of Fig. 8(a). The corresponding characteristic field is shown in Fig. 8(b), where region (1) remains elastic, and δ_2 is the angle between the crack line and the asymptote (oO'') of the new curved fan sector, region (6). As shown in Dong and Pan[14], $\theta_6 = 125.26°$ and $\delta_2 = 70.53°$. A total of fourteen equations are solved by Newton's method. The solutions for $M^e = 0.30$, $M^e = 0.15$, and $M^e = 0$ (mode II) are shown as the solid lines in Fig. 3. Again, the excellent agreement between the analytical solutions and the finite element results for all the cases is evident. The antisymmetric mode II near-tip field is shown in Fig. 8(c) for completeness. Note that *only* under pure mode II conditions, the elastic sector (1) becomes a plastic constant stress sector and the field becomes fully yielded at all angles.

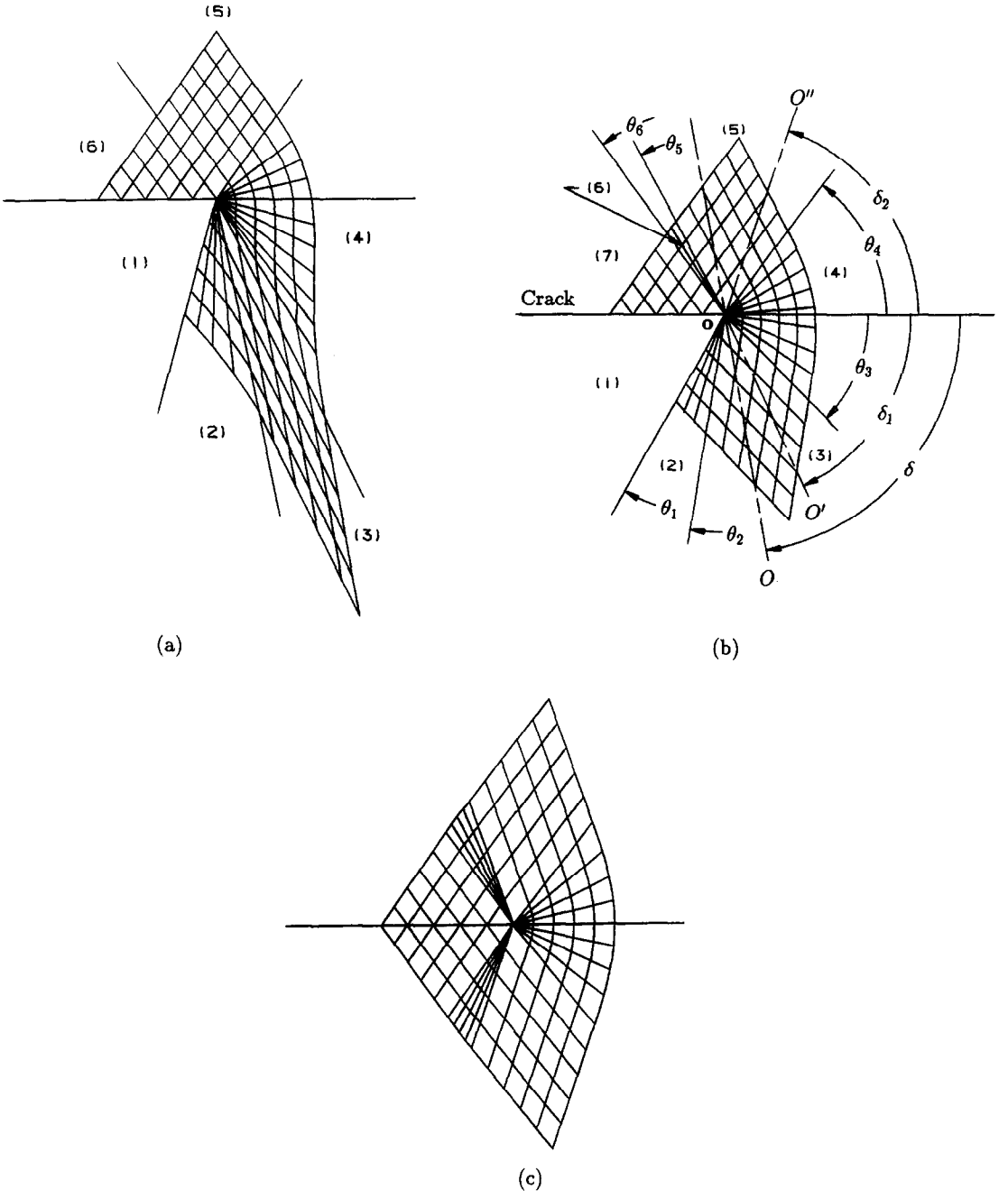

Fig. 8. Assembly of the crack-tip solutions under near mode II mixed-mode loadings: (a) the intermediate case between the near mode I and near mode II loadings, (b) near mode II mixed-mode loading, (c) pure mode II.

4. DISCUSSION

The current study under plane-stress mixed-mode conditions, along with the study under plane-strain mixed-mode conditions[12], consistently show that for elastic perfectly plastic materials, if the elastic part of the strain rate tensor is taken into account, it seems reasonable to introduce elastic sectors in the crack-tip fields. The radial lines across which the discontinuities in σ_{rr} occur, as envisioned in the rigid perfect-plasticity solutions, are actually replaced by elastic regions in the same neighborhoods. Under plane-strain conditions, there exists one elastic sector bordering the upper crack face in the near-tip fields for near mode I mixed-mode loading[12]. Under plane-stress conditions, there exists two elastic sectors bordering both crack faces for pure mode

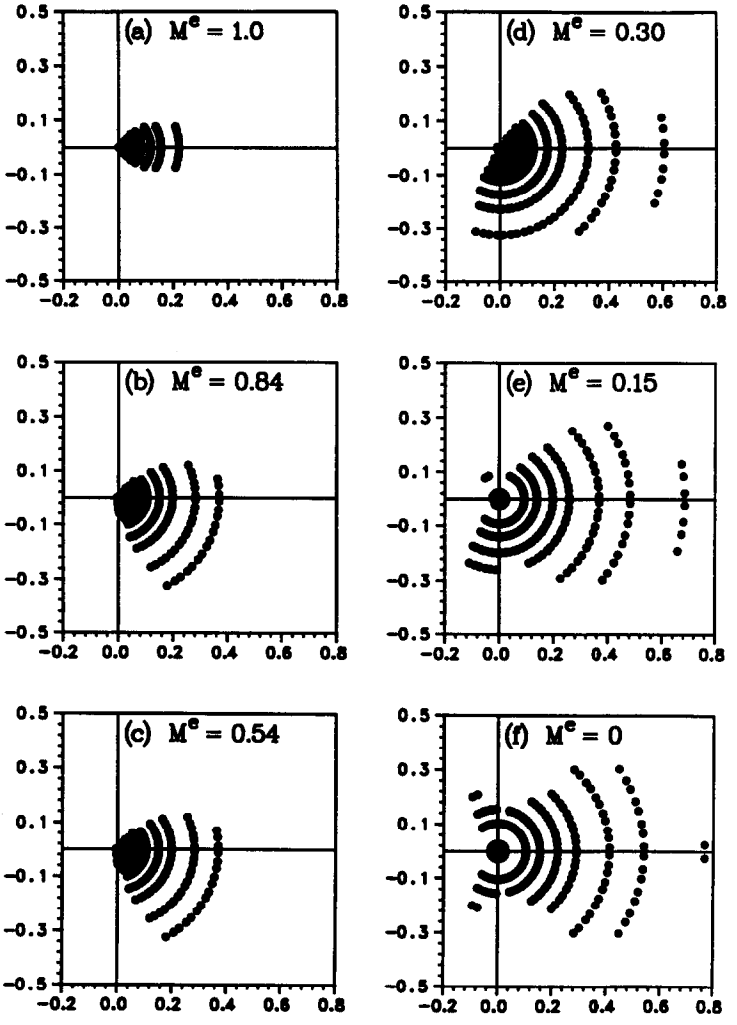

Fig. 9. Plastic zones plotted in the normalized coordinates by JE/σ_0^2: (a) $M^e = 1$ (mode I), (b) $M^e = 0.84$, (c) $M^e = 0.54$, (d) $M^e = 0.30$, (e) $M^e = 0.15$, (f) $M^e = 0$ (mode II).

I and near mode I mixed-mode loading, and one elastic sector bordering the lower crack face for near mode II mixed-mode loading. Within the elastic sectors, the stresses appear to be nonsingular under both plane-stress and plane-strain conditions[11, 12].

The normalized plastic zones from the current finite analysis are shown in Fig. 9 for different combinations of remote mixed-mode loadings. Each point in the figures represents a Gauss quadrature point in plastic state. The plastic zone sizes are consistently scaled by the self-similar parameter JE/σ_0^2 for all the cases, regardless of the remote loading levels, provided that the corresponding steady-state stress fields had been observed.

For all combinations of the remote mixed-mode loadings, the relationship between the near-field mixity M^e and the far-field mixity M^p is completely different from the relationship extrapolated from the power-law hardening solutions by Shih[5], while under plane-strain conditions the relationship between M^e and M^p is very close to the one extrapolated from power-law hardening solutions[12]. This demonstrates that under plane-stress conditions the material elasticity strongly influences the relation of the near-tip mixity to the far-field mixity, compared to that of the perfectly plastic solutions extrapolated from the solutions for power-law hardening materials[5]. This is in contrast to the plane-strain case, where the relation of the near-field mixity to the far-field mixity for perfectly plastic materials, extrapolated from the solutions for power-law hardening materials, is well-bounded by that for elastic perfectly plastic materials[5, 12].

It is worth noting that the constant stress sector [region (2) of Fig. 7(c)] is introduced to ensure the existence of solutions while the presence of it is not clearly indicated by the finite element results. Although the correlations between the near-tip fields for both plane stress and plane strain are not clear, it is natural to wonder if this has any implications on the near-tip fields for plane strain, since one possible solution suggested by Gao[9] has the same structure as the one shown in Fig. 7(b). Indeed, it appears that the arbitrariness of Gao's solutions[9] may be removed by arguing that a solution structure must be valid for the entire range of near mode I mixed-mode loading. Consequently, the slip-line field proposed by Saka *et al.*[10] should result (note that the solutions of Saka *et al.*[10] missed a constant stress sector when compared with those of [11, 12]). Apparently this issue has been bypassed in previous analyses[10, 11, 12], where the finite element computations clearly show that region (1) is a plastic constant stress sector.

Finally, it should be mentioned that the mode I solution shown in Fig. 7(a) is the mode I limit of the mixed-mode solutions. In fact, under the symmetric mode I loading the parameter θ_2 (or θ_3) is nonunique. A parametric study[20] has been conducted, and the results indicate that stress fields except σ_{rr} as functions of θ are virtually insensitive to the choice of the angular span $(\theta_2 - \theta_3)$ of the constant stress sector ahead of the crack tip, ranging from 1.83° to 20°. However, the finite element results suggest that the mode I solution should be either the case of the mode I limit of mixed-mode solutions or the case where the constant stress sector degenerates to a line (i.e. $\theta_2 = \theta_3 = 0$). Since there is little difference between the two corresponding stress fields for small values of θ_2 and θ_3, distinguishing one from the other with finite element methods proves to be difficult. Nevertheless, according to the arguments given in [21, 22, 23], it is reasonable to choose the case of the mode I limit of the mixed-mode solutions as the mode I crack-tip field under small-scale yielding conditions within the context of plane-stress theory. Investigations of the three-dimensional fields and the effects of tip blunting for a crack in a thin sheet subject to mode I loading can be found in [24, 25].

Acknowledgements—The authors acknowledge the support of the Nuclear Regulatory Commission under grant number NRC-04-87-113. JP also acknowledges the partial support of this work by the National Science Foundation under grant number MSM-8613544. Valuable discussions with the NRC program manager Mike Mayfield and Prof. C. F. Shih of Brown University during the course of this investigation are greatly appreciated.

REFERENCES

[1] J. W. Hutchinson, Singular behaviour at the end of a tensile crack in a hardening material. *J. Mech. Phys. Solids* **16,** 13–31 (1968).
[2] J. W. Hutchinson, Plastic stress and strain fields at a crack tip. *J. Mech. Phys. Solids* **16,** 337–347 (1968).
[3] J. R. Rice, A path independent integral and the approximate analysis of strain concentration by notches and cracks. *J. Appl. Mech.* **35,** 379–386 (1968).
[4] J. R. Rice and G. F. Rosengren, Plane strain deformation near a crack tip in a power law hardening material. *J. Mech. Phys. Solids* **16,** 1–12 (1968).
[5] C. F. Shih, Elastic-plastic analysis of combined mode crack problems. Ph.D. thesis, Harvard University, Cambridge, MA (1973).
[6] C. F. Shih, Small-scale yielding anaysis of mixed mode plane-strain crack problems, in *Fracture Analysis, ASTM STP* **560,** pp. 187–210. American Society for Testing and Materials (1974).
[7] J. Pan, Plane-strain crack tip stress field for anisotropic perfectly-plastic materials. *J. Mech. Phys. Solids* **34,** 617–635 (1986).
[8] J. Pan, Plane-stress crack-tip fields for perfectly plastic orthotropic materials. *Int. J. Fracture* **8,** 103–122 (1988).
[9] Y. C. Gao, Elastic-plastic field of a crack before growing in perfectly plastic medium (In Chinese). *Acta Solid Mech. Sinica* **1,** 69–75 (1980).
[10] M. Saka, H. Abé and S. Tanaka, Numerical analysis of blunting of a crack tip in a ductile material under small-scale yielding and mixed mode loading. *Comput. Mech.* **1,** 11–19 (1986).
[11] P. Dong and J. Pan, Near-tip fields in elastic perfectly plastic solids. ESP25.88022, Preprints 25 of the ASME/SES Conference, University of California, Berkeley, CA (20–22 June 1988).
[12] P. Dong and J. Pan, Plane-strain mixed-mode near-tip fields in elastic perfectly plastic solids under small-scale yielding conditions. *Int. J. Fracture* (in press).
[13] R. Narasimhan and A. J. Rosakis, A finite element analysis of small-scale yielding near a stationary crack under plane stress. SM Report 86-21, California Institute of Technology, Pasadena, CA (June 1986).
[14] P. Dong and J. Pan, Asymptotic crack-tip fields for perfectly plastic solids under plane-stress and mixed-mode loading conditions. *J. Appl. Mech.* (in press).
[15] T. Hughes, Generalization of selective integration procedures to anisotropic and nonlinear media. *Int. J. Numer. Meth. Engng* **15,** 1413–1418 (1980).
[16] K. J. Bathe and A. P. Cimento, Some practical procedures for the solution of nonlinear finite element equations. *Comput. Meth. Appl. Mech. Engng* **22,** 59–85 (1980).

[17] J. R. Rice, Elastic-plastic crack growth, in *Mechanics of Solids*: *The R. Hill 60th Anniversary Volume* (Edited by H. G. Hopkins and M. J. Sewell), pp. 539–562. Pergamon Press, Oxford (1982).
[18] L. M. Kachanov, *Fundamentals of the Theory of Plasticity*, pp. 244–262. Mir Publishers, Moscow (1974).
[19] R. Hill, On discontinuous plastic states, with special reference to localized necking in thin sheets. *J. Mech. Phys. Solids* **1**, 19–30 (1952).
[20] Z. E. A. Ben-Aoun and J. Pan, Plane-stress crack-tip fields for elastic pressure-sensitive plastic materials. (In preparation).
[21] P. Dong, Mixed-mode near-tip fields for elastic perfectly plastic solids. Ph.D. thesis, The University of Michigan, Ann Arbor, MI (1989).
[22] N. Nishimura and J. D. Achenbach, Finite deformation crack-line fields in a thin elasto-plastic sheet. *J. Mech. Phys. Solids* **34**, 147–165 (1986).
[23] P. F. Thomason, *Fracture Mechanics in Engineering Application* (Edited by G. C. Sih and S. R. Valluri), pp. 43–54. Sijthoff & Noordhoff, The Netherlands (1979).
[24] T. Nakamura and D. M. Parks, Conditions for J-dominance in three-dimensional thin cracked plates, in *Analytical, Numerical, and Experimental Aspects of Three Dimensional Fracture Processes* (Edited by A. J. Rosakis, K. Ravi-Chandar and Y. Rajapakse), AMD-Vol. 91, ASME, New York (1988).
[25] C. L. Hom and R. M. McMeeking, Crack tip blunting in thin ductile sheets, in *Analytical, Numerical, and Experimental Aspects of Three Dimensional Fracture Processes* (Edited by A. J. Rosakis, K. Ravi-Chandar and Y. Rajapakse), AMD-Vol. 91, ASME, New York (1988).

(*Received* 19 *June* 1989)